Journal of Magnetic Resonance 300 (2019) 18–27

Contents lists available at ScienceDirect

Journal of Magnetic Resonance

journal homepage: www.elsevier.com/locate/jmr

Normalized averaged range (nAR), a robust quantification method for MPIO-content

Maarten Naeyaert [a,*], Dimitri Roose [a], Zhenhua Mai [a], Aneta Keliris [a], Jan Sijbers [b], Annemie Van der Linden [a], Marleen Verhoye [a]

[a] Bio-Imaging Lab, University of Antwerp, Universiteitsplein 1, 2610 Wilrijk, Antwerp, Belgium
[b] imec-Vision Lab, University of Antwerp, Universiteitsplein 1, 2610 Wilrijk, Antwerp, Belgium

ARTICLE INFO

Article history:
Received 15 September 2018
Revised 6 December 2018
Accepted 20 December 2018
Available online 21 December 2018

Keywords:
MPIO
Quantification
Positive contrast
Stem cell tracking
Artefact reduction

ABSTRACT

Micron-sized paramagnetic iron oxide particles (MPIO) are commonly used as contrast agents in magnetic resonance imaging (MRI) that produce negative contrast enhancement, i.e. darkening, on $T2^*$-weighted images. However, estimation and quantification of MPIO in vivo is still challenging. This limitation mainly arises from smearing and displacement of the negative contrast of the MPIO, so-called blooming, potentially leading to false-positive detection. Further, the bias field induced by the MR coils also hinders visualization and quantification of the MPIO. To mitigate these drawbacks, a positive contrast image can be generated, for example by using a frequency offset technique, which can significantly improve the accuracy of quantification methods. In this research, we introduce the normalized average range (nAR) as a new way to quantify the relative MPIO content within a study. The method compares the average value of test ROIs to that of a control ROI in range filtered images. The nAR can be used on both positive and negative contrast images.

The nAR was tested on agar phantoms containing various MPIO concentrations, and on a rostral migration model for MPIO labeled stem cells in mice. The amount of MPIO was quantified for biased and unbiased data, and both for positive and negative contrast images. In addition, the presence of MPIOs in the olfactory bulb was verified by histology.

The results show the nAR can indicate the presence and relative content of MPIO for both negative and positive images. However, the nAR showed slightly higher sensitivity in optimized positive contrast images compared to negative contrast images. In all cases, the bias field played a minor role in the quantification, making debiasing less of a concern. The dependency of the nAR values on the MPIO content in the ROI was further validated histologically. Thus, the nAR provides a robust and reliable tool for quantification of MPIO in mice.

1. Introduction

Iron oxide nanoparticles are used as negative contrast-enhancing agents in magnetic resonance imaging (MRI) for multiple applications including imaging inflammation [1], liver imaging [2], drug delivery and therapy monitoring, and non-invasive cell tracking [3,4]. As superparamagnetic nanoparticles, they induce a local inhomogeneity in the magnetic field, which has a far greater influence on the transverse relaxation than on the longitudinal relaxation, resulting in a fast dephasing of the magnetic moments. Therefore, they produce excellent negative contrast on T_2^*-weighted images [5], i.e. they cause hypo-intense spots or regions in the image. Furthermore, it has been shown that micron-sized superparamagnetic iron oxide (MPIO) particles could generate single particle contrast at high resolution MRI [6]. However, due to off-resonance effects, the negative contrast does not exactly represent the size, shape and location of the superparamagnetic particles, which is referred to as the 'blooming artefact' [7]. Thus the sensitivity to detect the particles is very high, but the specificity in terms of localization and quantification of the amount of particles is low. Another issue is that negative contrast is less conspicuous than positive contrast. Over the last years, different methods were developed that aim to invert the T_2^* negative contrast to a positive contrast, such as gradient-compensating techniques, off-resonance techniques, and post-processing techniques [7–10]. All have their benefits and drawbacks, e.g. some need specially designed pulse sequences and therefore require additional anatomical scans. Recently, a positive contrast method was

* Corresponding author.
E-mail address: Maarten.Naeyaert@uantwerpen.be (M. Naeyaert).

https://doi.org/10.1016/j.jmr.2018.12.019
1090-7807/

established that uses off-resonance image datasets of radially sampled data [9,10], called Center-Out RAdial Sampling with Off-Resonance reception (CO-RASOR). The method is based on the physical effect that magnetic field disturbances cause signal pile-up near the field disturbance. By applying a specific frequency offset, the signal pile-up can be relocated to the center of the disturbance such that the specificity on the location of the particles is increased significantly. The method was first applied by repeatedly acquiring the data, with different frequency shifts applied [9], but further research aimed to develop an algorithm that applies the frequency offsets during image reconstruction [10]. This enables the acquisition of a single on-resonance scan, which improves time-efficiency and allows for greater flexibility to apply the frequency offset method. A slight variation of the CO-RASOR was used by Diwoky et al. [8], where the final positive contrast image was simply the voxelwise difference between the minimum and maximum signal over the frequency shifts applied.

Visualization and quantification of migrating MPIO labeled stem cells by MRI is a highly demanding MRI task since it requires a high-resolution acquisition, but it is very sensitive and even allows the detection of single voxels containing MPIO. The necessity for reliable detection and quantification of MPIOs comes from their great potential to be used as imaging markers (i.e. cell tracking) and carriers of pharmaceutical compounds [11–13] that could be tracked noninvasively by MRI. A variety of quantification methods have been reported in the literature for negative contrast images. One of those is SIRMA [14], which was designed for much higher concentrations than those used in this research. Machine learning has been used to automatically detect low MPIO concentrations in the mouse brain, but this method requires training data from different experiments and MPIO's that generate clear spots since they need to be labeled by a human operator beforehand [15]. Other MPIO quantification methods are the error-weighted difference [16,17] or the number of non-false positive outliers [4] between control and test Regions Of Interest (ROI's). These methods rely on the assumption that intensity of the ROI's is Gaussian-distributed, using the mean and standard deviation of the intensity histogram, and also require the ROI's to be of approximately equal size. The first condition prohibits their use as reliable quantification methods for positive contrast images, which are generally sparse, while the second condition could be an unnecessary hindrance. Thus, there is a need for a quantification method that either takes into account the intensity distribution of the positive contrast images or does not rely on the Gaussian distribution.

Another obstacle for reliable quantification is the bias field induced by the RF coil. RF coils have a non-uniform sensitivity and generally receive less signal from tissue further away from the coil, making those regions less bright. This effect is called the bias-field. Because of this, the intensity, contrast to noise and signal to noise ratio become dependent on the position with respect to the coil and thus the actual positioning of the patient or subject. In this way, the bias field interferes with the visualization and image quantification, segmentation or tissue classification in T_2^*-weighted images, together with the negative contrast produced by the MPIO. In general, surface coils induce a more severe bias field, but volume coils also suffer from it, and the magnitude and shape of the bias field are always dependent on the design of the coil. The bias field can be removed through various algorithms [18,19], usually by fitting a mathematical model to the data, but sometimes by measuring the bias field beforehand. It is possible that the bias-field and debiasing interfere with quantification methods, as they influence the intensity distribution [17]. This influence on the quantification should be estimated, and if possible, minimized or eliminated by choosing appropriate acquisition and reconstruction settings and quantification methods.

In this work, we propose the normalized Average Range (nAR) as a new way to quantify the relative MPIO content within and between images of a single experiment, based on comparing the texture between control and test ROIs, which we hypothesize to be highly correlated to MPIO presence in ROI's. The nAR is calculated by applying a range filter to a positive contrast image and measuring the ratio of the average range filtered values between test and control ROI's. The nAR was designed with positive contrast images in mind, but is also applicable on negative contrast images.

The quantification of MPIO content using the nAR was investigated on Cartesian T_2^*-weighted gradient echo images obtained from agar phantoms, and on ex-vivo images in a mouse model presenting migration of iron oxide particle labeled endogenous stem cells [3,4]. Both negative contrast images and positive contrast images, generated using CO-RASOR [10], were used for quantification. The efficacy of the quantification method was tested for different acquisition settings, and, in the case of positive contrast images, for different reconstruction settings. Additionally, the effect of the debiasing is investigated.

2. Material and methods

2.1. MPIO signal offset theory, reconstruction and post-processing

2.1.1. Theory

The principle of the frequency shift method is explained in detail by Seevinck and de Leeuw [9,10]. Briefly, as illustrated in Fig. 1a–d, a magnetic field disturbance induces a local frequency shift which can be described by [8,20]

$$\Delta f_{(r,\theta)} = \frac{\gamma}{4\pi}\frac{K_{Fe}m_c}{r^3}(3\cos^2\vartheta - 1) \quad (1)$$

where γ is the gyromagnetic ratio, 42.58 MHz/T [21], r is the distance from the MPIO, m_c is the iron mass load, K_{Fe} is a calibration constant [20], and θ is the angle between the B0 field and the vector along which r is measured. This altered frequency leads to a signal smear when the local field gradient is steeper than the intended frequency encoding gradient, and a signal pile-up in the other case, as illustrated in Fig. 1d. A larger MPIO cluster will have a larger iron mass load, and thus a larger frequency shift.

This effect manifests itself only in the frequency encoded direction. The magnitude of the signal displacement for a Cartesian acquisition scheme, expressed as the number of voxels shifted, is given by [8]

$$\Delta\bar{x}_{RO} = \frac{\Delta f_{(r,\theta)}N}{BW}\bar{e}_{RO} \quad (2)$$

Here N is the number of voxels in the read-out direction, $\bar{e}_{RO}$ is the unity vector of the read-out direction, and BW is the total bandwidth along the read-out direction. This signal displacement is what causes the blooming artefact, and hides the size and exact location of the field perturbance.

2.1.2. Positive contrast image generation using the offset method

Positive contrast images, wherein most of the background is suppressed but MPIO are bright and well localized, can be constructed out of the T_2^* weighted images by combining several frequency offset images. A detailed explanation can be found in [10], but the idea is explained schematically in Fig. 1e–h. Briefly, by applying positive and negative frequency offsets, subtracting each frequency offset image from the original $T2^*$ image and averaging the results, the signal pile-up can be shifted to the center of the disturbance. Because the optimal frequency offset is dependent on the local MPIO concentration, multiple frequency offsets could be needed to reposition the different MPIO accumulations in a

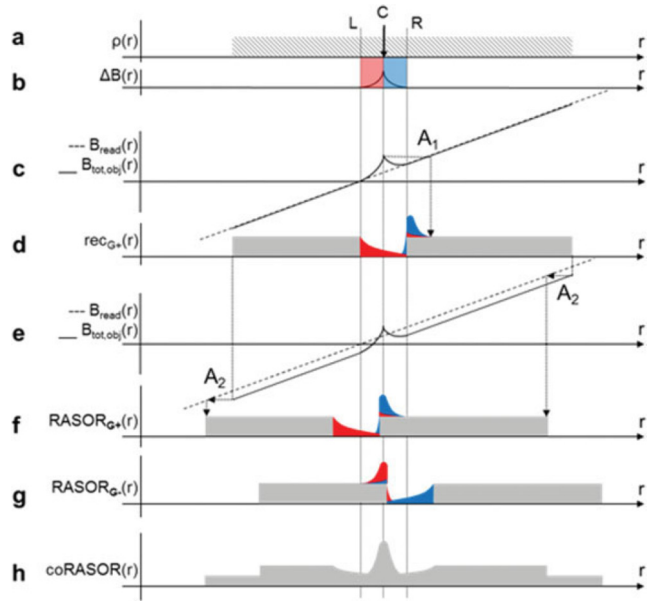

Fig. 1. A 1D schematic representation of the reconstruction principle. An object with constant spin density ρ(r) (gray hatched area) is depicted in (a), containing a small paramagnetic field perturber at location C. When placed in a magnetic field, the field perturber induces a nonlinear magnetic field distortion (ΔB), as schematically depicted in (b). A positive field gradient is induced between the edges L and C, as highlighted in red, while a negative field gradient is induced between the edges C and R, as highlighted in blue. In (c), the dotted line represents the linear magnetic field (B_{read}) related to a positive read gradient (G+). The black line represents the total magnetic field ($B_{tot,\ obj}$) in the object, which is a summation of $B_{read}(r)$ and ΔB (r). At locations where the intended and true field gradients do not coincide, the spatial encoding is disturbed, as depicted in the reconstructed intensity profile in (d). Arrow A1 demonstrates the erroneous spatial encoding of signal in the direct vicinity of the field perturber. In (e), a frequency offset is applied during reconstruction, represented by an upward shift of the entire read gradient-related field B_{read} (dotted line). This causes the entire object to shift to the left, as shown in (f) and pointed out by arrows A2. The frequency offset is taken such that the blue signal pile-up in (d) is repositioned at the exact center of the field perturber (location C in a). Similarly, when using a negative read gradient (G–) the red area from (d) will pile-up. This piled-up signal can also be repositioned at the exact center of the field perturber, resulting in the intensity profile as depicted in (g). By averaging the positive and negative read gradients, as is done in co-RASOR (h), high positive contrast at the exact center of the field perturber is obtained (adapted from [10]). (For interpretation of the references to colour in this figure legend, the reader is referred to the web version of this article.)

subject [22]. To be certain all MPIO concentrations get reconstructed well, the frequency offsets are applied in different increments, called the step size, until the maximal frequency offset, also called offset range, is reached. Both of these parameters are user-defined, and their influence will be investigated.

The frequency offsets were applied by multiplying the complex k-space data with a frequency ramp $e^{-i2\pi\delta f_0|r|}$ with δf_0 the frequency offset and r the distance from the center of k-space before reconstruction. The offsets were applied using Matlab (The MathWorks, Natick, MA) based on the original code kindly provided by Hendrik de Leeuw [10]. Although the acquisition in our study is based on a Cartesian sampling scheme, the frequency ramp is applied radially.

2.1.3. Quantification method using the normalized average range (nAR)

An MPIO quantification method based on a texture filter was developed which can in principle be used on both negative and positive contrast images since it does not assume a Gaussian intensity distribution. First, a range filter, which calculates the difference between the largest and smallest value in a $3 \times 3 \times 3$ window, is applied over the whole positive contrast image. If a region is very smooth, the range will be very small. If the texture is rough and contains many bright spots, however, the range in a region will be large. To detect MPIO in a test ROI, the Normalized Average Range (nAR) is defined as:

$$nAR_i = \frac{\langle r_i \rangle}{\langle r_c \rangle} - 1 \tag{3}$$

where $\langle r_c \rangle$ and $\langle r_i \rangle$ denote the average value of the range filtered image for a control ROI, and the i-th ROI respectively. If a control ROI containing no MPIO is selected, a nAR equal to 0 indicates the absence of MPIO in a ROI, and higher values indicate more MPIO are present in a ROI.

This method imposes a few constraints, namely that the control and test ROIs should have a similar SNR, since the range value can also be used as a noise estimator for a smooth surface. Furthermore, a ROI should be sufficiently large so as not to be affected by noise.

2.2. Phantom construction

Agar phantoms with MPIOs were prepared to test the method and investigate the influence of several acquisition and processing parameters. The phantom constituted of four 0.5 ml tubes (Eppendorf AG, Hamburg, Germany) each containing a mixture of agar gel (1% agar, A9539, Sigma-Aldrich, St Louis, MO, USA) and a different concentration of blue fluorescent MPIO particles (glacial blue, cat no. ME04F/7833, Bangs Laboratories, Fishers, IN, USA). The particles were sonicated before being transferred to the Eppendorf tubes to ensure a homogeneous distribution throughout the agar, after which the tubes were further filled with agar. The Eppendorf tubes were then put into a larger container filled with distilled water. To test the quantification method over a larger range of concentrations and to test the consistency of the quantification, two phantoms were made with 'high' concentrations of MPIO, and two were made with 'low' concentrations. The high concentration phantoms had four tubes containing pure agar, or an MPIO/agar solution with ratios of 1/2000, 1/4000 or 1/8000**,** while the low concentration phantoms contain tubes filled with agar, or 1/8000, 1/16000 and 1/32,000 dilutions of MPIO. The iron content for each solution was calculated using information obtained from the website of the manufacturer, and by using the data found in [6]. The different iron contents are listed in Table 1.

2.3. In vivo cell labeling

Endogenous neural stem cell (eNSC), residing in the brain's subventricular zone, were labeled with blue fluorescent MPIO particles (glacial blue, cat no. ME04F/7833, Bangs Laboratories, Fishers, IN, USA) through a stereotactic intraventricular injection (2.7×10^7 particles; 3.00 mg Fe/ml). In vivo cell labeling was performed as previously described [4]. Six mice were anesthetized by intraperitoneal injection with a mixture of ketamine (Anesketin: 100 mg/ml; Eurovet NV/SA, Heusden-Zolder, Belgium) and medetomidine (Domitor: 1 mg/ml; Pfizer Animal Health s.a., Louvain-la-Neuve, Belgium), and positioned in a stereotactic head frame. Stereotactic

Table 1
The iron content for each dilution used in the phantom experiments.

MPIO dilution	Iron content
1/2000	1,537,650 pg/ml
1/4000	768,825 pg/ml
1/8000	384,413 pg/ml
1/16000	192,206 pg/ml
1/32000	96,103 pg/ml

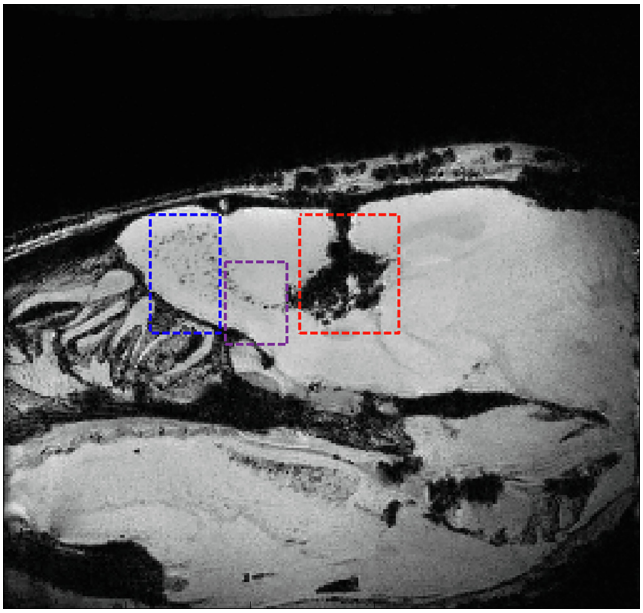

Fig. 2. Debiased T_2^* weighted MRI image illustrating the MPIO labeled stem cell migration from the injection site in the subventricular zone (red box, right), via the RMS (purple box, middle) to the olfactory bulb (blue box, left). MPIO can be seen as black dots. The injection site is small in reality, but the high concentration of MPIO's causes a significant blooming artefact. (For interpretation of the references to colour in this figure legend, the reader is referred to the web version of this article.)

coordinates (relative to bregma) for the right ventricle injection were: anterior 1 mm – lateral 0.75 mm – dorsal 2.3 mm. A Hamilton syringe (26 S Gauge, VWR International, Haasrode, Belgium) was connected with a pump to inject the MPIO particles at a constant rate of 0.50 µl/min. After MPIO injection, the needle was left in place for an additional 5 min and then slowly withdrawn. After surgery, anesthesia was reversed using atipamezole (Antisedan 5 mg/ml, Pfizer Animal Health s.a) administered subcutaneously. The eNSC, both labeled and unlabeled, migrate spontaneously but slowly along the rostral migration stream (RMS), causing an accumulation of MPIO at the olfactory bulb, the endpoint of the RMS.

Fig. 2 illustrates the migratory path of the MPIO labeled eNSC. Fifteen weeks after MPIO-labeling, after the eSNC and MPIO have been passed through the migration stream [4], mice were sacrificed for *ex vivo* MRI with an intraperitoneal overdose of pentobarbital (Nembutal; CEVA Santé Animale, Brussels, Belgium) and transcardially perfused with 4% paraformaldehyde (PFA) in 0.1 M PBS (pH 7.4). Then, the mouse heads were fixed overnight in 4% PFA at 4 °C prior to transfer to PBS. All surgical interventions were approved by the ethical committee for animal experiments of the University of Antwerp (dossier 2009-33) and were performed in accordance with all the guidelines and regulations.

2.4. Magnetic resonance imaging acquisition

Imaging of phantoms and mice was performed on a Bruker Pharmascan 7 T imaging system with a horizontal bore (Bruker, Ettlingen, Germany). Each of the four phantoms was scanned on two independent imaging sessions. The phantom images were acquired using a volume transmission coil and a rat-brain quadrature receiver-only surface coil. The phantom images were acquired using a T_2^* weighted gradient echo sequence of which the standard settings were as follows: TE = 8 ms, TR = 100 ms, flip angle 18°, field of view (FoV) = (30 × 30 × 17) mm^3, matrix = (384 × 384 × 218), 78 µm isotropic voxel size, receiver bandwidth = 29,761 Hz, read out direction head-foot and 3 averages, taking about 7 h.

Since the size of the frequency offset depends on several user-controlled parameters as can be seen in Eqs. (1) and (2), the phantoms were scanned repeatedly during a single session using varying acquisition strategies, based on the standard settings described above. This was done in order to gain information about potential optimal acquisition settings and to investigate the robustness of the quantification method. The different acquisition settings were: 1) standard setting; 2) increased bandwidth to 59,523 Hz; 3) shortened TE = 5.5 ms with BW = 59,523 Hz; 4) lower resolution (256 × 256 × 145 matrix); 5) reversed read-out direction (foot-head instead of head-food); 6) read out direction left-right; 7) standard scan settings using only one average. This last scan was used to check the stability of the phantom and the influence of SNR.

The ex-vivo images were acquired by scanning the mouse heads (N = 6) using a receive-only mouse brain surface RF coil and using a volume coil for transmission. A high-resolution 3D T_2^*-weighted GE sequence was applied with the following imaging settings: TR = 100 ms, TE = 8 ms, 22° flip angle, FoV = (17 × 17 × 17) mm^3, matrix = (256 × 256 × 256), 66 µm isotropic voxel size, six averages and a receiver bandwidth of 50,000 Hz, with a total scan time of approximately 11 h [4].

2.4.1. ROIs in the phantoms

For quantification in the phantoms, a ROI was drawn for each Eppendorf tube using Amira (FEI Company, Hillsboro, OR, USA) by selecting a circular region near the top and bottom of a tube and interpolating between these circles. This resulted in the selection of a ROI in the shape of a truncated cone. ROI edges were placed away from the edges of the Eppendorf tube to avoid the inclusion of any possible acquisition or reconstruction artefacts, such as inhomogeneities from small air bubbles.

2.4.2. Spatial normalization and ROIs in ex-vivo images

In order to quantify the MPIO in the images, two ROIs were selected in the olfactory bulb for all animals, on the contra- and ipsilateral side of the MPIO injection, respectively the control and test ROI. First, a population-based atlas was constructed using the Advanced Normalization Tools (ANTs) [23], by spatially normalizing the debiased 0 Hz offset dataset of 3 mice, which corresponds to the original magnitude image dataset. Secondly, a rectangular ROI was delineated in the ipsilateral olfactory bulb on the atlas and this ROI was mirrored to the contralateral olfactory bulb using Matlab. Lastly, the mouse-to-atlas transformation matrix was calculated for all 6 animals using ANTs, and both ROIs were back-transformed into the native space of the original mouse datasets.

2.5. Influence of positive contrast reconstruction parameters

To study their influence, the frequency step size and maximal frequency offset used in the positive contrast image generation were varied both for the phantom and the ex-vivo images. Since the manner in which the MPIO's aggregate and cluster is different in the agar phantoms compared to stem cells [22], the optimal settings could be different and the procedure was repeated for both studies. The influence of the reconstruction parameters of the positive contrast images on the MPIO quantification using the average range per ROI can be investigated clearly using the phantom. Meanwhile, the ex-vivo images provide the opportunity to investigate how the surrounding responds to different settings, and whether this causes any interference with the MPIO detection. For the phantoms, the step sizes used were 10 Hz, 20 Hz, 50 Hz and 100 Hz, while the frequency ranges were 50 Hz, 100 Hz, 250 Hz, 500 Hz and 1000 Hz. If a certain frequency range could

not be made using a certain step size (e.g. range of 50 Hz using step sizes of 20 Hz) the positive contrast image for those settings was not created. For the ex-vivo images, the offset frequency ranges were 50 Hz, 100 Hz, 250 Hz, 500 Hz, 1000 Hz, 2000 Hz and 5000 Hz and the step sizes which were tested were 10 Hz, 50 Hz, 250 Hz and 500 Hz, at an offset range of 500 Hz.

2.6. Influence of bias field and debiasing

To assess the influence of the bias field introduced by the non-uniform sensitivity of the surface RF coil on the quantification of positive contrast images, the same procedure was done for both biased and debiased datasets, starting with the calculation of the offset images up to the quantification. To generate the unbiased positive contrast image, the 0 Hz image was debiased using the N4 bias field correction [24]. Offset images and positive contrast images were created starting from the debiased 0 Hz images, as described in the previous section for biased images.

2.7. Statistics

In the ex-vivo images, a single sample Wilcoxon signed rank test was used to determine whether the median of the nAR was different from zero using SPSS 23 (IBM, Armonk, NY, USA). A two way repeated measures ANOVA was used between the biased and debiased images and between the positive contrast and negative contrast images to test if the mean nAR was different, i.e. if there was a relatively increased accuracy, again using SPSS.

2.8. Histology

Two mice, one showing significant MPIO migration and one showing sparse to no migration according the nAR values, were processed for histology as previously described in [22], to correlate MRI findings with the histological outcome. Whole brains were surgically removed and freeze-protected by passing through a sucrose gradient (2 h at 5%, 2 h at 10% and overnight at 20%) after which they were frozen in liquid nitrogen and stored at −80 °C until further processing for immunofluorescence. Consecutive 10 µm-thick cryosections were prepared from the olfactory bulb using a microm HM500. MPIO were counted manually in a representative subset of slices from the olfactory bulb using fluorescence microscopy.

3. Results

3.1. Phantom results

3.1.1. Detecting different MPIO concentrations in positive and negative contrast images

The nAR values of the biased positive contrast images of all different MPIO concentrations of all the phantoms are presented in Fig. 3A. A maximal frequency offset and step size of 100 Hz and 10 Hz respectively were used to construct the positive contrast images. The lines are linear interpolations between the three MPIO concentrations for each phantom separately. In all cases, a higher MPIO concentration gave a higher nAR value, although the slope between phantoms is different. The nAR was able to detect iron concentrations of lower as 1 ng/ml, a concentration which was very difficult to detect by the human eye.

Fig. 3b shows the mean of the nAR values of the positive and negative contrast measurements, both for the biased and debiased images, and a linear interpolation for each case in the range of MPIO solution dilutions between 1/32,000 and 1/2000, representing concentrations of ~1–16 ng/ml (Table 1). It can be seen that

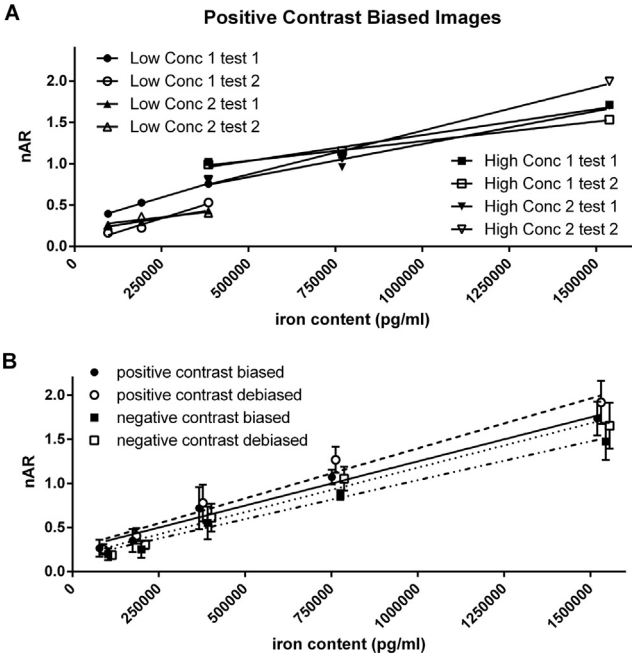

Fig. 3. (A) The influence of different MPIO concentrations on the nAR in biased positive contrast images using a step size of 10 Hz and a maximal frequency offset of 100 Hz. All measurements of all phantoms are included, and linear interpolations between the nAR values are shown for each phantom separately. (B) Mean nAR values and errors for biased and debiased, and positive and negative contrast images, and linear interpolations between the data. Positive contrast images were generated using a step size of 10 Hz and a maximal frequency offset of 100 Hz. The nAR can detect MPIO in positive and negative contrast images, and both for biased and debiased data, but lower values nAR values are detected in negative contrast and biased data.

the nAR is able to discriminate between MPIO concentrations and has a linear response to the iron content in all cases, but lower values are detected in biased and in negative contrast images, and the nAR difference between concentrations is larger in debiased images.

3.1.2. Testing the nAR in positive contrast images

3.1.2.1. Maximal frequency offset and frequency step size variation for phantoms

A visual example of the influence of the maximal offset frequency on the positive contrast reconstruction can be seen in Fig. 4. Choosing a higher maximal frequency offset improves the SNR, but also brings about artefacts, such as widening the edges of the container and shading of the tube edge, best seen when maximal offset frequency = 1000 Hz. The influence of the maximum frequency offset on the measured nAR is shown in Fig. 5A. Although the choice of the maximal frequency offset can diminish the resolving power somewhat, the nAR is relatively robust against variations of the frequency offset range.

The effect of the step size on the nAR in positive contrast phantom images using a maximal frequency offset of 100 Hz is shown in Fig. 5B. The step size has almost no effect on the magnitude of the nAR, and only a very slight increase can be observed when the step size increases for all concentrations. Visually the reconstructions look very similar (results not shown).

3.1.2.2. Different acquisition strategies

The influence of the acquisition parameters on the nAR is shown in Fig. 6. The low resolution scan scores best, yielding higher detection values and a better resolving power between ROIs. However,

Fig. 4. The influence of the maximum offset frequency on the positive contrast reconstruction of a phantom with low MPIO concentrations. The MPIO content and the position of the ROIs is indicated. The original negative contrast image is in the top left, maximal offset frequency is indicated for the other images. For all positive contrast images step size = 10 Hz.

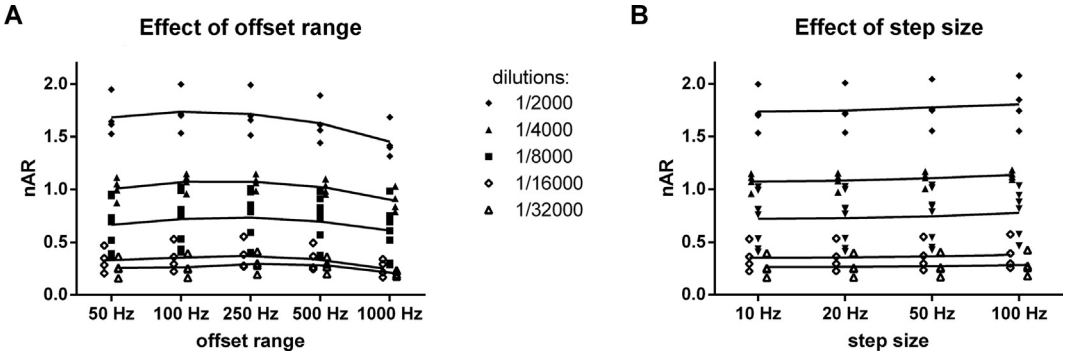

Fig. 5. The influence of the frequency offset range and step size on the nAR in biased positive contrast images: All individual points are indicated. The solid lines connect the mean values for each concentration. (A) The influence on the maximal frequency offset for images reconstructed with frequency step size = 10 Hz. (B) The influence of the frequency step size in images reconstructed with maximal offset frequency = 100 Hz.

the error is relatively large for these measurements. The standard acquisition and reversed read-out gradient sense acquisition result in similar nAR values. Choosing a lower TE resulted in lower nAR values in all cases. Using a higher bandwidth lowered the nAR in the high concentration phantoms. The low SNR scan, which only uses one average instead of three, also has clearly lower detection values for both types of phantom.

3.2. Results for the ex-vivo scans

3.2.1. Maximal frequency offset and optimal step size for animals

While testing if MPIO could be detected in the animal model, the effect of the maximal frequency offset and the frequency step size was also tested. To test the maximal frequency offset, the nAR in the biased ex-vivo images was calculated for positive contrast reconstructions using a step size of 10 Hz but with varying frequency offset ranges. These results are shown in Fig. 7. There is a very clear effect of the maximal offset frequency on the nAR, with 500 Hz giving the largest difference between test and control ROI. One animal did not seem to have taken up MPIO in the olfactory bulb, and showed an almost constant value of about 0, decreasing for larger maximal offset ranges. As in the phantoms, the frequency step size only has a minimal effect on the nAR (results not shown).

3.2.2. Quantification of MPIO in ex vivo images

For quantification, the nAR was calculated on positive contrast images reconstructed using a step size of 50 Hz and a frequency range of 500 Hz, and on the original negative contrast images. The procedure was done for both the biased and debiased images. The results for all individual animals and their mean are shown in Fig. 8A. Animal 6 was not included in this mean, as the nAR

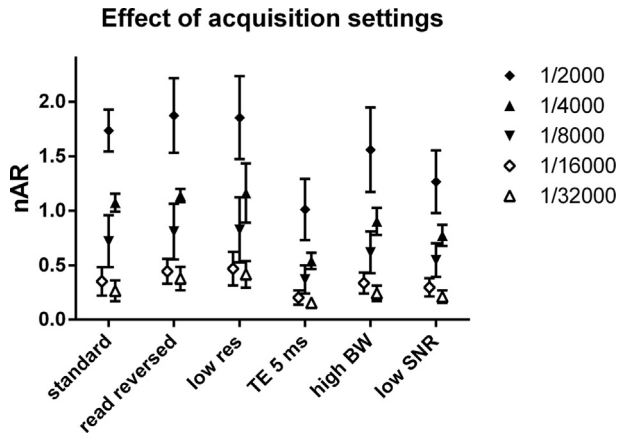

Fig. 6. The influence of acquisition settings on the nAR in biased positive contrast images reconstructed with step size = 10 Hz and maximal offset frequency = 100 Hz.

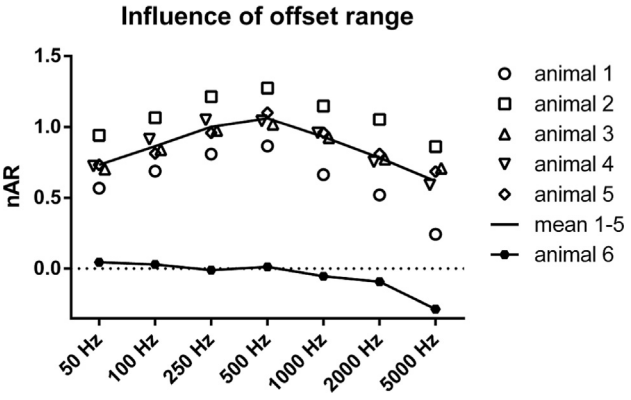

Fig. 7. Ex-vivo results for the influence of the maximal offset frequency on the nAR, using step size = 10 Hz. Individual points are shown, while the full line shows the mean nAR value of all animals that demonstrated MPIO presence in the olfactory bulb. Animal 6 was not included when calculating the mean, as it was confirmed by histology that no MPIO were present in the olfactory bulb in this animal.

indicated no MPIO were present in the olfactory bulb. Histology was done on animal 6 to confirm if this was indeed the case.

For both biased and debiased positive contrast images the Wilcoxon signed rank test indicated that the median of the nAR was not equal to 0, with p = 0.028. Because of the low sample size and using a rank-based test, the possible p-values are discretized, thus leading to an equal p-value for both tests. The values range from nAR = 0.83–1.05 for the debiased images and nAR = 0.87–1.27 for the biased images.

In the negative contrast images, the Wilcoxon signed rank test still indicated that the median was not equal to one, for the biased results again with p = 0.028, for the debiased results p = 0.046. The values range from nAR = 0.53–0.85 for the biased negative contrast images and nAR = 0.48–0.67 for the debiased images.

The ANOVA to test whether measuring the nAR was significantly changed in biased versus debiased or positive versus negative contrast images found that this is the case for positive versus negative contrast images (p = 0.004), but not for biased versus debiased images (p = 0.305). A significant interaction effect was found (p = 0.021). A representative example of negative and positive contrast, and biased and debiased ex-vivo images is provided in supplementary image 2.

3.2.3. Histology

In the ex-vivo images, 5 out of 6 animal olfactory bulbs showed a high nAR value, while one animal showed a low nAR value. Histology on this animal and on one animal having a high nAR value confirmed that the increase in nAR is caused by MPIO presence in the test ROI. The MPIO present in the olfactory bulb were counted in the exemplary histological slices using the previously described method [22]. The preliminary histological results confirmed our MRI findings, namely the animal showing nAR = 0.01 had only 20 MPIO, while another mouse with nAR = 1.27 had 162 MPIO in the evaluated slices. The nAR values reported are for the biased positive contrast data reconstructed using a frequency offset range of 500 Hz and a frequency step size of 50 Hz.

4. Discussion

A novel method to quantify the relative amount of MPIO in a T_2^* weighted MRI image was presented. The method calculates the normalized average value of an intensity range filtered positive contrast image for test ROIs with regard to a control ROI, with the control ROI containing no MPIO. Positive contrast images were generated to refocus the MPIO clusters to a more correct size and location. The frequency offsets which are applied to generate the positive contrast image were determined by an offset step size and offset range chosen by the user. Phantoms containing different MPIO concentrations were used to test whether the nAR was able to detect the relative MPIO presence, to investigate how the nAR was influenced by the step size and offset range, and to determine the influence of acquisition settings and of the bias field, and of debiasing during preprocessing. The results indicate that the nAR is able to detect low concentrations of iron and has a linear response to iron concentrations in the range

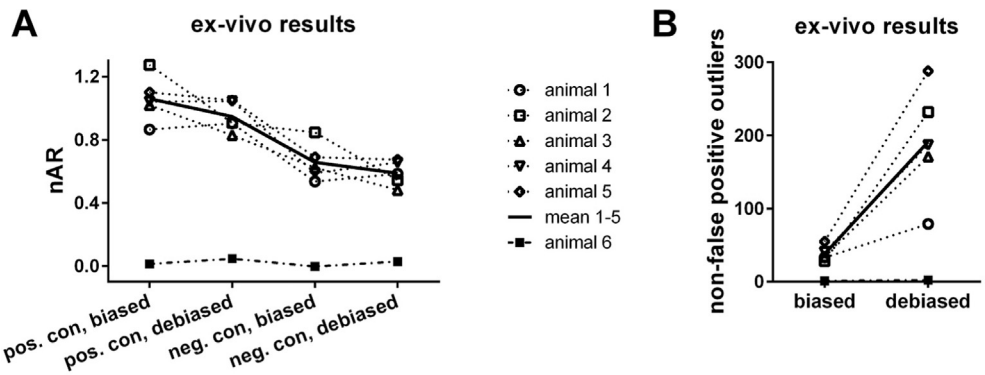

Fig. 8. (A) nAR values for the positive and negative contrast ex-vivo images, both the biased and the debiased versions. The positive contrast images were reconstructed with frequency step size = 50 Hz and maximal offset frequency = 500 Hz. Animal 6 was not included in the mean because it gave very deviating results. (B) The same data quantified by counting the number of non-false positive outleirs in the negative contrast images.

used in this research, ~1–16 ng/ml (Table 1). The method was also verified on ex-vivo images of MPIO labeled stem cells in the olfactory bulb of mice, and the step size, offset range and importance of debiasing were again investigated. Histology confirmed that the nAR value is correlated to the MPIO content of the olfactory bulb. While the nAR is sensitive to inhomogeneities, it is not specific as to what causes them, and air bubbles in the phantoms, for example, can also cause a high nAR. This can be avoided by excluding recognizable unwanted inhomogeneity sources from the ROIs.

Although MPIO presence and relative concentrations were detected correctly for all cases, several factors appeared to have a limited influence on the nAR and its sensitivity and resolving power between MPIO concentrations upon investigation.

4.1. Positive versus negative contrast images

When negative contrast images are used, the nAR values are consistently lower as in the positive contrast images, indicating a lower sensitivity. In the ex-vivo measurements, the difference between positive and negative contrast images is larger as in the phantoms. The improved conspicuity of MPIO in positive contrast images is thus reflected in the nAR values, and producing the positive contrast images is a valuable step in the processing of T_2^* weighted images to detect and quantify MPIO, especially for lower iron concentrations.

4.2. Effect of frequency offset range and step size

When using the nAR on positive contrast images, the frequency offset range is the parameter with the most influence on the nAR value for both the phantoms and the ex-vivo images. Although the nAR has the same general behavior in both the phantom and ex-vivo data when varying the offset range, the dependency on the offset range of the nAR was larger in the ex-vivo images as in the phantom images. Formula (2) allows for a reasonable first guess for the frequency range. The reason for the existence of an optimal offset range value can be explained by considering the tradeoff between an offset which is high enough to cover all relevant MPIO concentrations and pinpoint their size and location, but not so high as to allow excessive blurring of edges or susceptibility artefacts in the positive contrast image. The reason for having different optimal frequency offset ranges between the phantoms and ex-vivo images is probably a combination of different factors, such as the different bandwidth and resolution used, the different types of edges in the background which show up in the positive contrast images, and the difference in MPIO clustering behavior between the 'homogeneous' phantoms and in labeled stem cells, where it has been shown that multiple MPIO can be contained in a single cell [22].

The positive contrast image and the nAR are less influenced by the step size of the frequency offsets. Since the MPIO are supposed to be homogeneously distributed throughout the phantoms, the offset artefact should be about equal in size for all MPIO particles, being influenced only by size distribution of the individual MPIO and iron content. In the ex-vivo images, clusters of different size are more likely to be present [22], and thus the step size could theoretically have a more noticeable effect since different iron concentration can be present in different voxels. However, this was not observed. Choosing a lower step size, however, will not have any detrimental effect except for a higher need for memory and a longer reconstruction time. It is thus prudent to choose a step size which is rather too low than too high.

4.3. Effect of acquisition settings

As could be inferred from Eqs. (1) and (2), certain acquisition parameters could have an influence on the artefacts caused by inhomogeneities and the nAR. As expected changing the sense of the read-out direction does not have an effect, but lowering the bandwidth has a detrimental effect. Changing the direction of the read-out gradient should have an effect, but due to fold-over artefacts of the water tube outside the field of view which could not be suppressed, this could not be investigated. Lowering the resolution but taking a higher number of averages improved the detection, somewhat surprisingly, but this can probably be attributed to the higher SNR of this acquisition. The SNR of the low-resolution scan is improved with a factor 1.53 because 7 averages instead of 3 were used, and a factor 3.38 because of the higher voxel volume when compared to the standard scan, for a total SNR improvement of 5.16. A standard scan with only one average had a reduced nAR, showing that SNR plays a role in the nAR value found. As explained in the method section, the range filter also acts as a noise detector, and SNR should be comparable between ROIs.

The TE should be chosen to get a good contrast of the MPIO particles. In the ex-vivo images, most of the recommendations which are clear from the phantom experiments were followed, except for the bandwidth, which was not changed from the standard setting and leading to a 2.5 times higher BW/pixel. Nonetheless, MPIO were still clearly detected in the ex-vivo case.

4.4. Effect of the bias field

Debiasing slightly increased the nAR values within a ROI in the phantoms, slightly improving the resolving power. However, in the ex-vivo images the nAR decreased slightly after debiasing, although no statistically significant result between the biased and debiased results were found for the ex-vivo images. The nAR is thus certainly robust with regard to the bias field for a ROI of limited size as was used in the ex-vivo case. There is not sufficient data to do a meaningful statistical test on the phantom data. The different response to debiasing is likely explained by the extent of the phantom ROI, which traverses a considerable part of the bias field and thus might be affected more, while this was not the case in the smaller ROIs of the ex-vivo images. Fig. S1 Shows the result of a phantom experiment whereby the nAR was determined for slices at different levels of the bias field, indicating that there is a noticeable but limited effect of the bias field on the quantification which remains unchanged after debiasing.

For completeness, the number of non-false positive outliers was counted in the negative contrast ex-vivo images for both the biased and debiased images, and the results are shown in Fig. 8B. The number of non-false positive outliers is determined by counting the number of voxels with an intensity lower than the mean minus two standard deviations for both ROIs, and subtracting this number of voxels in the contralateral ROI (false positives) from the number of voxels found in the ipsilateral ROI (false positives plus non-false positives) [4]. Although the animal containing no MPIO is clearly distinguished from the other animals, it can be seen that this type of analysis is much more sensitive to the bias field and debiasing as the nAR.

4.5. Shortcomings and possible extensions

This study has some shortcomings. The nAR is not an absolute quantification method, as the resolving power between MPIO levels is dependent on several acquisition and reconstruction parameters, somewhat similar to the ADC value in diffusion MRI. However, the method reliably detects differences within an image, and between images acquired and processed using identical procedures. The nAR is also designed to quantify low concentrations of MPIO, where the clusters or particles are localized in a mostly homogeneous background. It is not designed to quantify MPIO if the concentrations and distribution are that high to cause a

general, homogeneous change in contrast or signal intensity. For example, in Fig. 2, it can be used to quantify the MPIO content in the blue and green rectangles, but not in the red rectangle, where the high MPIO concentrations causes an extensive signal void. Furthermore, only a single type of MPIO were used in this research. In principle the nAR should be sensitive to the contrast generated by other types of particles, but this has not yet been tested.

Since the goal of the research was to investigate the behavior of the nAR in phantoms using different acquisition strategies and on high–resolution ex-vivo-images, the total scan time was very long. The method can - in principle - also be applied for in vivo acquisitions, as shown in [4]. While a faster scan protocol was not tested, a lower resolution scan with more repetitions was very capable of detecting the MPIO content using the nAR, and a high-resolution but low SNR experiment showed that even with lower SNR, MPIO could be detected. Using a smaller FoV, fewer repetitions but a lower resolution, it should be possible to use this technique in vivo as well, but further research is needed to validate this claim.

The frequency offset method was originally designed for radially sampled k-space data. Therefore, the method was slightly modified so it could be applied to k-space data sampled with a Cartesian scheme. Applying the frequency offset only along the read-out direction resulted in hard to interpret images because edges are only detected in one direction, and the noise becomes correlated along the direction of the applied frequency shifts. Applying a frequency shift dependent on the radial distance from the center results in homogeneous noise and edge enhancement, but at the price of slightly less focused particles. Although the sampling and thus the inhomogeneity sensitive direction was different from De Leeuw et al., some of their findings were also observed in our study [10]. They showed for example that their method works best on symmetrical objects. This is also observed in our data: the MPIO that still reside at the site of injection, which can be considered as a single field perturbing object with an asymmetrical shape, are not well reconstructed since the signal pile-up is not relocated to the center of the object. Furthermore, they also observed that only a single well-chosen frequency offset is needed to generate a positive contrast image. Although multiple steps were used in this research to be certain no MPIO or MPIO clusters were overlooked, due to their varying sizes and iron contents, the results in Fig. 5 show no dependence on the step size for all frequency ranges tested, indicating that a single step could suffice, if it is well chosen.

Other methods to estimate the MPIO signal in negative contrast images exist, such as calculating the error weighted difference [16,17] or counting the number of non-false positive outliers [4]. These methods were not used in this study because they assume a Gaussian intensity distribution in the ROIs, which is not the case in positive contrast images, and because they require that ROIs are very similar in size, which was perceived as a drawback, and because they suffer from shortcomings similar to the nAR, which makes their use as a validation tool in this setting very limited. The non-false positive outliers were checked for the ex-vivo data, but only to see how sensitive this method is to debiasing. Using machine learning to detect MPIO is possible, but requires a priory MPIO labels, decided by humans, and thus MPIO which are clearly visible [15]. The method presented here was able to detect MPIO presence even at very low concentrations where the human eye could not reliably detect their presence.

5. Conclusion

The nAR is a reliable way to detect MPIO presence. Iron concentrations of 1 ng/ml could be detected repeatedly in phantom experiments, and nAR indicated MPIO presence in five animals containing MPIO, and MPIO absence in one animal which was confirmed not to have MPIO by histology. Although the nAR found the correct iron concentration differences in all cases, the sensitivity could be improved by using optimized acquisition settings and by using positive contrast images for quantification, reconstructed using an optimized frequency offset range. The nAR value is largely insensitive to the step size used for the positive contrast reconstruction. The effect of debiasing depends on the extent and location of the ROIs used but is mostly limited. Although able to give an indication of the MPIO content for different measurements within an experiment, the nAR is not a real quantification method, as its value depends on several acquisition and reconstruction settings. The nAR values between different experiments should not compared.

Acknowledgments

We wish to thank dr. Jörn Engelmann for his invaluable help and advice regarding the design and construction of the phantoms, and Dr. H. De Leeuw for providing the original CO-RASOR code. Furthermore, we wish to thank prof. Erik Shapiro at the department of Radiology of Michigan State University for providing additional info about the particle iron content, and Dr. Steven Joosen at the Systemic Physiological and Ecotoxicological Research (SPHERE) laboratory of the University of Antwerp for his help in determining whether the iron content could be measured experimentally.

This work was supported by the interdisciplinary PhD grant (ID) UA BOF-DOCPRO 2010 [granted to S. Bals, P. Ponsaerts, A. VdL.] and the interdisciplinary PhD grant (ID) UA BOF-DOCPRO 2012 [granted to M.V.]; and further partially supported by funding received from: the European Union's Seventh Framework Programme (grant FP7/2007-2013; INMiND) [grant agreement 278850, granted to AVdL.], the molecular Imaging of Brain Pathophysiology (BRAINPATH) [grant FP7-PEOPLE-2013-IAPP-612360], by the Hercules stichting [grant agreement no. AUHA/012], financing MRI-research infrastructure. None of the funding sources had any influence on the design or conduct of the study.

Appendix A. Supplementary material

Supplementary data associated with this article can be found, in the online version, at https://doi.org/10.1016/j.jmr.2018.12.019.

References

[1] B.C. te Boekhorst, G.A. van Tilborg, G.J. Strijkers, K. Nicolay, Molecular MRI of inflammation in atherosclerosis, Curr. Cardiovasc. Imaging Rep. 5 (2012) 60–68, https://doi.org/10.1007/s12410-011-9114-4.

[2] D.D. Stark, R. Weissleder, G. Elizondo, P.F. Hahn, S. Saini, L.E. Todd, J. Wittenberg, J.T. Ferrucci, Superparamagnetic iron oxide: clinical application as a contrast agent for MR imaging of the liver, Radiology 168 (1988) 297–301, https://doi.org/10.1148/radiology.168.2.3393649.

[3] E.M. Shapiro, O. Gonzalez-Perez, J. Manuel García-Verdugo, A. Alvarez-Buylla, A.P. Koretsky, Magnetic resonance imaging of the migration of neuronal precursors generated in the adult rodent brain, Neuroimage 32 (2006) 1150–1157, https://doi.org/10.1016/j.neuroimage.2006.04.219.

[4] R. Vreys, G. Vande Velde, O. Krylychkina, M. Vellema, M. Verhoye, J.P. Timmermans, V. Baekelandt, A. Van der Linden, MRI visualization of endogenous neural progenitor cell migration along the RMS in the adult mouse brain: validation of various MPIO labeling strategies, Neuroimage 49 (2010) 2094–2103, https://doi.org/10.1016/j.neuroimage.2009.10.034.

[5] Y. Gossuin, P. Gillis, A. Hocq, Q.L. Vuong, A. Roch, Magnetic resonance relaxation properties of superparamagnetic particles, Wiley Interdiscip. Rev. Nanomedicine Nanobiotechnol. 1 (2009) 299–310, https://doi.org/10.1002/wnan.36.

[6] E.M. Shapiro, S. Skrtic, K. Sharer, J.M. Hill, C.E. Dunbar, A.P. Koretsky, MRI detection of single particles for cellular imaging, Proc. Natl. Acad. Sci. USA 101 (2004) 10901–10906, https://doi.org/10.1073/pnas.0403918101.

[7] W. Liu, H. Dahnke, E.K. Jordan, T. Schaeffter, J.A. Frank, In vivo MRI using positive-contrast techniques in detection of cells labeled with superparamagnetic iron oxide nanoparticles, NMR Biomed. 21 (2008) 242–250, https://doi.org/10.1002/nbm.1187.

[8] C. Diwoky, D. Liebmann, B. Neumayer, A. Reinisch, F. Knoll, D. Strunk, R. Stollberger, Positive contrast of SPIO-labeled cells by off-resonant reconstruction of 3D radial half-echo bSSFP, NMR Biomed. 28 (2015) 79–88, https://doi.org/10.1002/nbm.3229.
[9] P.R. Seevinck, H. de Leeuw, C. Bos, C.J.G. Bakker, Highly localized positive contrast of small paramagnetic objects using 3D center-out radial sampling with off-resonance reception, Magn. Reson. Med. 65 (2011) 146–156, https://doi.org/10.1002/mrm.22594.
[10] H. de Leeuw, P.R. Seevinck, C.J.G. Bakker, Center-out radial sampling with off-resonant reconstruction for efficient and accurate localization of punctate and elongated paramagnetic structures, Magn. Reson. Med. (2012), https://doi.org/10.1002/mrm.24416.
[11] C.W. Lu, J.K. Hsiao, H.M. Liu, C.H. Wu, Characterization of an iron oxide nanoparticle labelling and MRI-based protocol for inducing human mesenchymal stem cells into neural-like cells, Sci. Rep. 7 (2017) 1–12, https://doi.org/10.1038/s41598-017-03863-x.
[12] S. Boutry, R.N. Muller, S. Laurent, Targeted iron oxide (nano)particles used as MRI contrast agent in small animal models, in: Iron Oxide Nanoparticles Biomed. Appl., Elsevier, 2018, pp. 135–164. https://doi.org/10.1016/B978-0-08-101925-2.00005-X.
[13] A.V. Naumova, G. Vande Velde, Genetically encoded iron-associated proteins as MRI reporters for molecular and cellular imaging, Wiley Interdiscip. Rev. Nanomed. Nanobiotechnol. 10 (2018), https://doi.org/10.1002/wnan.1482.
[14] F. Franconi, C. Chapon, J.J. Le Jeune, P. Richomme, L. Lemaire, Susceptibility gradient quantization by MRI signal response mapping (SIRMA) to dephaser, Med. Phys. 37 (2010) 877–884, https://doi.org/10.1118/1.3298019.
[15] M.J. Afridi, A. Ross, X. Liu, M.F. Bennewitz, D.D. Shuboni, E.M. Shapiro, Intelligent and automatic in vivo detection and quantification of transplanted cells in MRI, Magn. Reson. Med. 78 (2017) 1991–2002, https://doi.org/10.1002/mrm.26571.
[16] C. Guglielmetti, J. Praet, J.R. Rangarajan, R. Vreys, N. De Vocht, F. Maes, M. Verhoye, P. Ponsaerts, A. Van der Linden, Multimodal imaging of subventricular zone neural stem/progenitor cells in the cuprizone mouse model reveals increased neurogenic potential for the olfactory bulb pathway, but no contribution to remyelination of the corpus callosum, Neuroimage 86 (2014) 99–110, https://doi.org/10.1016/j.neuroimage.2013.07.080.
[17] G. Vande Velde, J. Raman Rangarajan, R. Vreys, C. Guglielmetti, T. Dresselaers, M. Verhoye, A. Van der Linden, Z. Debyser, V. Baekelandt, F. Maes, U. Himmelreich, Quantitative evaluation of MRI-based tracking of ferritin-labeled endogenous neural stem cell progeny in rodent brain, Neuroimage 62 (2012) 367–380, https://doi.org/10.1016/j.neuroimage.2012.04.040.
[18] U. Vovk, F. Pernus, B. Likar, A review of methods for correction of intensity inhomogeneity in MRI, IEEE Trans. Med. Imaging 26 (2007) 405–421, https://doi.org/10.1109/TMI.2006.891486.
[19] Z. Hou, A review on MR image intensity inhomogeneity correction, Int. J. Biomed. Imaging 2006 (2006) 1–11, https://doi.org/10.1155/IJBI/2006/49515.
[20] C.V. Bowen, X. Zhang, G. Saab, P.J. Gareau, B.K. Rutt, Application of the static dephasing regime theory to superparamagnetic iron-oxide loaded cells, Magn. Reson. Med. 48 (2002) 52–61, https://doi.org/10.1002/mrm.10192.
[21] P.J. Mohr, D.B. Newell, B.N. Taylor, CODATA recommended values of the fundamental physical constants: 2014, Rev. Mod. Phys. 88 (2016) 035009, https://doi.org/10.1103/RevModPhys.84.1527.
[22] D. Roose, F. Leroux, N. De Vocht, C. Guglielmetti, I. Pintelon, D. Adriaensen, P. Ponsaerts, A. Van der Linden, S. Bals, Multimodal imaging of micron-sized iron oxide particles following in vitro and in vivo uptake by stem cells: down to the nanometer scale, Contrast Media Mol. Imaging 9 (2014) 400–408, https://doi.org/10.1002/cmmi.1594.
[23] B.B. Avants, P.T. Schoenemann, J.C. Gee, Lagrangian frame diffeomorphic image registration: morphometric comparison of human and chimpanzee cortex, Med. Image Anal. 10 (2006) 397–412, https://doi.org/10.1016/j.media.2005.03.005.
[24] N.J. Tustison, B.B. Avants, P.A. Cook, Yuanjie Zheng, A. Egan, P.A. Yushkevich, J. C. Gee, N4ITK improved N3 bias correction, IEEE Trans. Med. Imaging 29 (2010) 1310–1320, https://doi.org/10.1109/TMI.2010.2046908.